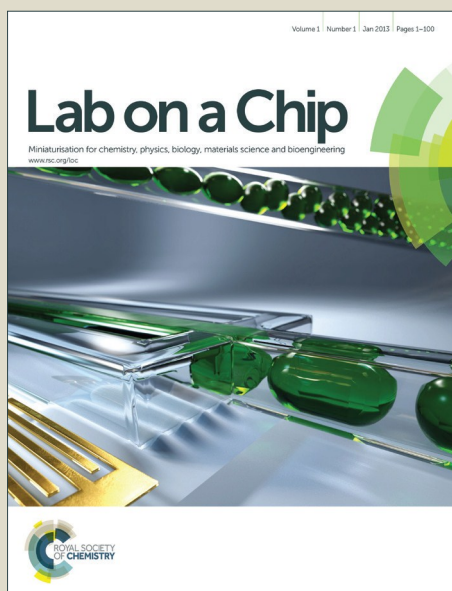


# Lab on a Chip

Accepted Manuscript



This is an *Accepted Manuscript*, which has been through the Royal Society of Chemistry peer review process and has been accepted for publication.

*Accepted Manuscripts* are published online shortly after acceptance, before technical editing, formatting and proof reading. Using this free service, authors can make their results available to the community, in citable form, before we publish the edited article. We will replace this *Accepted Manuscript* with the edited and formatted *Advance Article* as soon as it is available.

You can find more information about *Accepted Manuscripts* in the [Information for Authors](#).

Please note that technical editing may introduce minor changes to the text and/or graphics, which may alter content. The journal's standard [Terms & Conditions](#) and the [Ethical guidelines](#) still apply. In no event shall the Royal Society of Chemistry be held responsible for any errors or omissions in this *Accepted Manuscript* or any consequences arising from the use of any information it contains.



Journal Name

ARTICLE

## On-chip microtubule gliding assay for parallel measurement of Tau protein species

Subhathirai Subramaniyan Parimalam,<sup>a</sup> Mehmet C. Tarhan,<sup>bc</sup> Stanislav L. Karsten,<sup>cd</sup> Hiroyuki Fujita,<sup>c</sup> Hirofumi Shintaku,<sup>a</sup> Hidetoshi Kotera,<sup>a</sup> and Ryuji Yokokawa<sup>a\*</sup>

Received 00th January 20xx,  
Accepted 00th January 20xx

DOI: 10.1039/x0xx00000x

www.rsc.org/

Tau protein is a well-established biomarker for a group of neurodegenerative diseases collectively called tauopathies. So far, clinically relevant detection of tau species in the cerebrospinal fluid (CSF) cannot be achieved without immunological methods. Recently, it was shown that different tau isoforms including their ones carrying various types of mutations affect MT-kinesin binding and velocity in isoform specific manner. Here, based on these observations we developed a microfluidic device to analyze tau mutations, isoforms and their ratios. The assay device consists of three regions: A MT reservoir captures microtubules (MTs) from the solution to the kinesin-coated surface. A microchannel guides gliding MTs, and an arrowhead shape collector concentrates MTs. Tau-bound fluorescently labeled MTs (tau-MTs) were assayed, and the increase of fluorescent intensity (FI) corresponding to the total number of MTs accumulated was measured at the collector. We show that our device is capable of differentiating 3R and 4R tau isoform ratios and effect of point mutations within 5 minutes. Furthermore, the radially oriented collector regions enable the simultaneous FI measurements for six independent assays. Performing parallel assays in the proposed device with minimal image processing provides a cost-efficient, easy-to-use and fast tau detection platform.

### 1 Introduction

An early and differential diagnosis of neurodegenerative diseases is essential for an effective therapeutic intervention and for the management of the disease outcome. The presence of distinct tau pathology specific to each tauopathy makes this protein an important differential biomarker.<sup>1,2</sup> Six tau isoforms are expressed in the neurons, and they differ according to the number of microtubule binding repeats (MTBRs; R1-R4 repeats) at C-terminal region and the length of the projection domain (ON-2N) at the N-terminal region.<sup>3</sup> The levels of cerebrospinal fluid (CSF) total tau,<sup>4</sup> phospho-tau<sup>5</sup> and the tau isoform ratio<sup>6</sup> (3R:4R) are evaluated in order to characterise the intracellular pathology.

Currently, immuno-based methods such as the enzyme-linked immuno sorbent assay (ELISA) have been used to clinically detect CSF-tau species.<sup>7,8</sup> The immuno-based method has been further developed by combining it with the two-photon Rayleigh scattering technique, in order to demonstrate highly sensitive CSF-tau detection.<sup>9</sup> Non-immuno detection, based on electrochemical impedance spectroscopy,<sup>10</sup> and capillary electrophoresis-based enzymatic reaction have also been reported.<sup>11</sup> However, since standardized clinical

procedures have not been well developed and established for a reliable CSF-tau detection,<sup>12</sup> alternative methods are in high demand.

Recently, a microtubule (MT)-kinesin based transport system has been successfully validated for tau detection in two assay geometries. (i) In a Lab-on-a-Chip compatible kinesin motility assay, the kinesin velocity was assayed on tau-bound MTs (tau-MTs) to differentiate various tau species. To increase the assay's sensitivity, tau-MTs were suspended between the micro-scale walls.<sup>13</sup> However, this method had a complex experimental setup and a long turnaround time (TAT) for multiple data processing. (ii) In a MT gliding assay, tau-MTs were assayed over a kinesin-coated surface using three parameters: MT landing rate, density, and gliding velocity were used to differentiate tau species. The MT landing rate and MT density were defined as the number of MTs that landed per unit time per unit area and the number of surface-attached MTs per unit area, respectively.<sup>14-17</sup> We previously reported a MT gliding assay based on tau specific interference on the MT-kinesin interaction.<sup>18</sup> In brief, the interference was mainly defined by their MT binding properties, such as the binding affinity,<sup>3</sup> the steric effect of MTBRs<sup>19</sup> and the protein conformation of tau when it binds to MT surface.<sup>20</sup> We demonstrated that MT-kinesin interaction is inhibited by 4R tau isoforms consequently lowering MT's affinity for the kinesin-coated surface together with their gliding capacity. Based on this previously established role of tau protein in MT gliding assays,<sup>15,18,21</sup> we designed a microfluidic device in an attempt to efficiently differentiate various tau species.

<sup>a</sup> Department of Micro Engineering, Kyoto University, Kyoto, Japan

<sup>b</sup> Laboratory for Integrated Micro Mechatronic Systems (LIMMS), Institute of Industrial Science (IIS), The University of Tokyo, Tokyo, Japan

<sup>c</sup> Center for International Research on Micronano Mechatronics (CIRMM), Institute of Industrial Science (IIS), The University of Tokyo, Japan

<sup>d</sup> NeuroInDx Inc., Signal Hill, CA, USA

Journal Name

ARTICLE

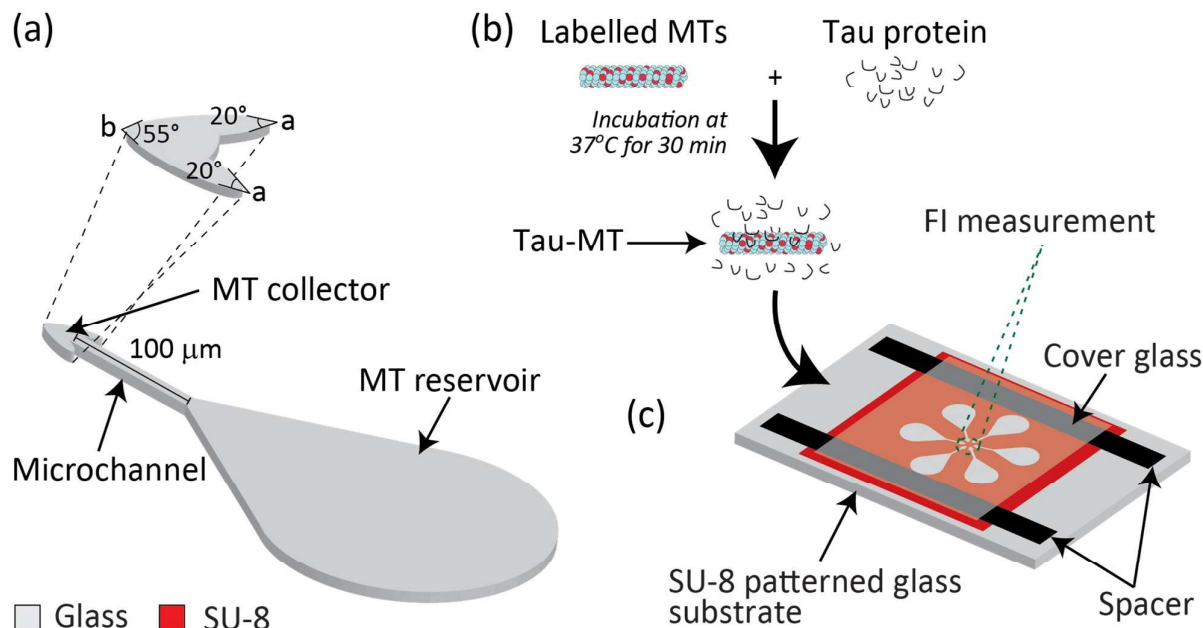


**Fig. 1.** Schematic representation of a) Microfluidic device comprising of MT reservoir, microchannel and MT collector. Angles of the MT collector,  $a=20^\circ$  and  $b=55^\circ$ , are defined as shown in the enlarged schematic. b) Preparation of tau-MT. c) Overview of the six assay units radially patterned for simultaneous measurement of MT accumulation at all the six collectors.

## Materials and Methods

### Design of the tau detection device

We designed a microfluidic device with an assay region comprising of a MT reservoir ( $24 \times 10^4 \mu\text{m}^2$  in area) and an arrowhead shape MT collector ( $175 \mu\text{m}^2$  in area, angle  $a=20^\circ$  and  $b=55^\circ$ ), and a microchannel connecting the reservoir and the collector ( $100 \mu\text{m}$  in length and  $5 \mu\text{m}$  in width) (Fig. 1a). In addition, an overhang structure was designed circumscribing the entire assay region to prevent MTs from leaving the kinesin-coated surface.<sup>25</sup> A single chip has six assay units oriented radially with collectors pointing towards the centre, and a flow cell was constructed for injecting solutions (Fig. 1c). The reservoir should be as large as possible to capture many MTs on the kinesin-coated surface. However, owing to the limited area to locate six units radially, the area was designed as  $24 \times 10^4 \mu\text{m}^2$ . This shape for guiding MTs to the microchannel was partly adopted from Lin et al. 2008.<sup>22</sup> The arrowhead collector was designed to efficiently concentrate MTs. Previously, arrowhead shape structures were incorporated in parallel<sup>26</sup> and circular microchannels<sup>27</sup> as a rectifier to achieve unidirectional MT gliding. This idea was

referred in our design, and only the inlet was connected to the microchannel to keep MTs gliding within the collector. To visualise all six collectors in a single frame under a fluorescent microscope and to detect as six independent fluorescent intensities, collectors were separated by a distance of  $15 \mu\text{m}$  and the area was designed as  $175 \mu\text{m}^2$ . The angle at the base of the arrowhead was designed as  $a=20^\circ$  and the tip angle was  $b=55^\circ$  for each collector.

The channel width was selected to be  $5 \mu\text{m}$ <sup>22,27</sup> to prevent MTs from making U-turns<sup>28</sup> and to guide them towards the collector. The length was designed as  $100 \mu\text{m}$  for MTs to reach a collector  $\sim 100 \text{ s}$  (gliding velocity of  $\text{MT} \sim 1 \mu\text{m s}^{-1}$ ) that enabled an assay within a few minutes. In addition, the selected length enabled to enhance the difference of MT gliding velocities, which was measured in the increase of fluorescent intensity (FI).

Based on the device design, when a solution containing MTs was introduced, it was expected that kinesins immobilized in the MT reservoir would capture MTs from the solution.<sup>22</sup> The capture efficiency of the reservoir would directly be affected by the amount and type of tau proteins bound to MTs owing to the difference in their landing rate and density.<sup>18</sup> The captured MTs would glide through the microchannel towards

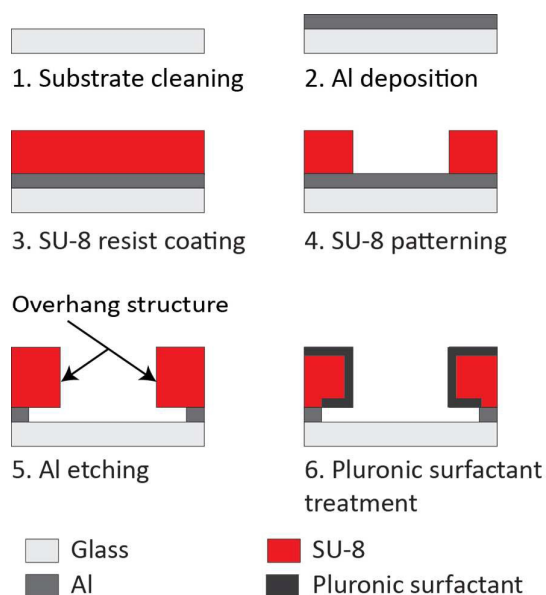


**Fig. 2.** Microfluidic device fabrication and Pluronic surfactant treatment.

the collector and be concentrated for FI measurement. Through the MT gliding in the channel, velocity difference according to tau species would be enhanced.<sup>15,18</sup> Therefore, the number of MTs reaching the collector would be determined by their capacity to bind and glide over the kinesin-coated surface. This results in the difference in FIs after a given assay time.

#### Fabrication of the tau detection device

A glass substrate (24 mm × 36 mm, No. 1 thickness Matsunami Glass) was cleaned using piranha solution ( $\text{H}_2\text{SO}_4:\text{H}_2\text{O}_2 = 3:1$ ) at 80°C for 20 min (Fig. 2). Then, 150 nm aluminium (Al) was deposited on the substrate (VPC-260F, ULVAC). A negative photoresist, SU-8 3005 (Microchem), was spun (6000 rpm, 30 s, 1-μm-thick film) on the Al-coated glass substrate, exposed through a photomask to UV light at the optimum dose of 51 mJ cm<sup>-2</sup>, developed in a SU-8 developer and rinsed in isopropanol. The overhang structure was created following as previously established fabrication process.<sup>28</sup> In brief, following the removal of the Al layer from the assay region, Al underlying the SU-8 was over-etched for the overhang structure. Al etching was carried out just prior to the tau detection assay to preserve the clean glass surface.

#### Selective kinesin patterning in the microfluidic device

A flow cell (Fig. 1c) was created over the microfluidic device using a cover glass (12 mm × 18 mm; Matsunami Glass) and paraffin tape as spacers (12.7 μm in thickness, Bemis, Parafilm M). Two glasses were sandwiched together on a hot plate at 120°C for 1 min to melt the paraffin and glue the glasses, leaving the other two sides open for fluid exchange. Before introducing the protein solutions into the device, nonspecific kinesin binding was eliminated by pre-treating the device with

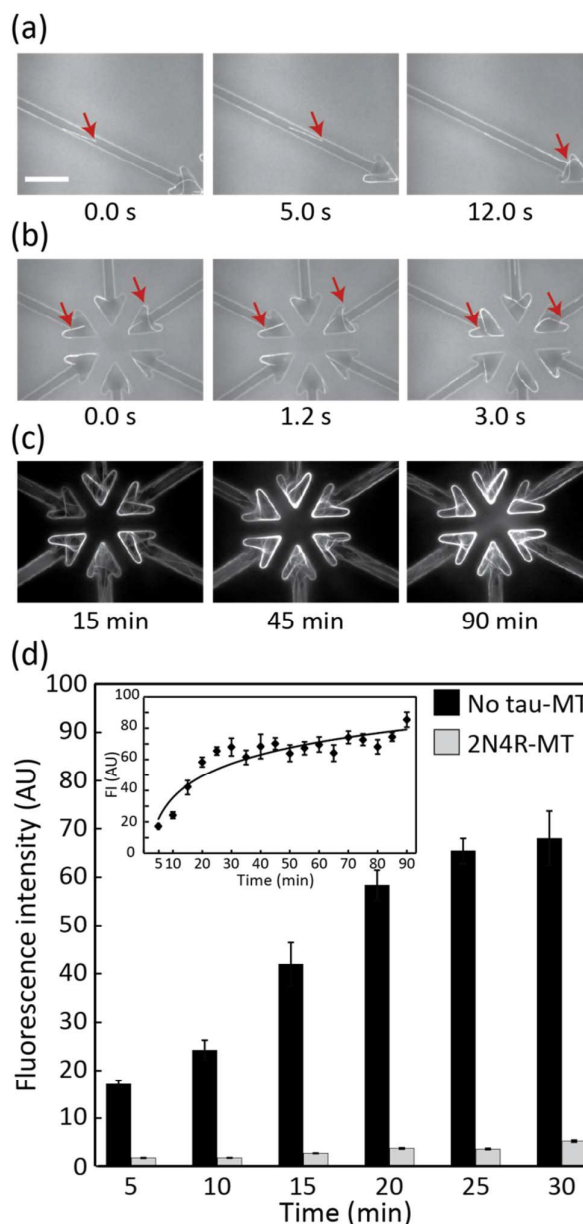


**Fig. 3.** MT motility and accumulation in the collector region in a microfluidic device. a) Sequential images of a MT gliding in a channel towards collector. b) MTs recirculated within collectors. c) MTs concentrated in collectors at 15, 45 and 90 min. Scale bar, 20 μm. d) FI of 2N4R-MT and no tau-MT. 2N4R-MT collector showed a significantly lower FI (t-test:  $p < 0.001$  mean ± SEM), and difference was significant 5 min after introducing MTs. Inset represents the FI profile of no tau-MT at the collector for 90 min.

a Pluronic surfactant (2 mg ml<sup>-1</sup>), which is a triblock polymer consisting of poly(ethylene oxide) – poly(propylene oxide) – poly(ethylene oxide) (PEO-PPO-PEO). The PEO chain formed a hydrophilic and protein repelling interface on the SU-8 (hydrophobic) surface. It blocked kinesin binding to the SU-8 surface.<sup>29</sup> On the contrary, the glass surface (assay region) was

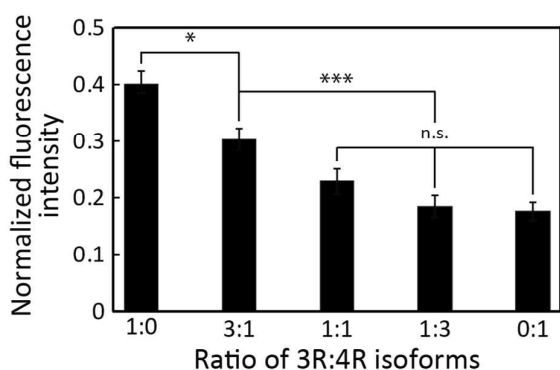


**Fig. 4.** Differentiation of different 2N3R:2N4R isoforms. Fls decreased with the increase of 2N4R tau. Mean  $\pm$  SEM; \*\*\*:  $p < 0.001$ ; \*:  $p < 0.05$ ; n.s.:  $p > 0.05$  (ANOVA);  $n \geq 12$ .

left hydrophobic to immobilise kinesin. The microfluidic device was thoroughly rinsed with DI H<sub>2</sub>O and BRB80 before the assay.

#### Preparation of proteins

Kinesin and tubulin protein preparations are described elsewhere.<sup>30,31</sup> In brief, recombinant *Homo sapiens* kinesin (amino acid residues 1–573) was expressed, isolated and purified from *Escherichia coli* Rosetta (DE3), then stored in liquid nitrogen (LN<sub>2</sub>). BRB80 containing 80 mM KOH-PIPES (piperazine-N, N'-bis (2-ethanesulfonic acid)), 1 mM MgCl<sub>2</sub> and 1 mM EGTA (ethylene glycol tetraacetic acid) was used as buffer solution for the entire experiments. Kinesin solution was prepared by diluting to 30  $\mu\text{g ml}^{-1}$  in BRB80 containing 2.5  $\text{mg ml}^{-1}$  casein, 1 mM ATP, and 1 mM MgCl<sub>2</sub>. Tubulin was purified from porcine brains obtained from a local slaughterhouse (Ikeda Food, Kyoto, Japan) by two cycles of assembly-disassembly procedure and phosphocellulose chromatography. A portion of the tubulin preparation was labeled with tetramethyl rhodamine (C1171, Molecular Probes) by standard protocols.<sup>32</sup> Tubulin was stored in LN<sub>2</sub> until use. MTs were polymerized from fluorescently labelled tubulin and unlabelled tubulin (1:10 molar ratio) at 37°C for 30 min in BRB80 buffer containing 1 mM MgSO<sub>4</sub> and 1 mM GTP. Polymerized MTs were stabilized by 40  $\mu\text{M}$  paclitaxel and used within 1–2 days after polymerization. Recombinant tau proteins (lyophilized in 50 mM, MES buffer) purchased from rPeptide were resuspended in DI H<sub>2</sub>O and stocked at –80°C.

For the tau detection assay, paclitaxel (10  $\mu\text{M}$ ) stabilized MTs (5  $\mu\text{M}$ ) were prepared and sheared for 30–35 times by a needle (22S gauge, 51 mm in length, Hamilton) to obtain a uniform distribution in MT length  $8.5 \pm 2.6 \mu\text{m}$ . Tau-MT solutions were prepared by incubating tau isoforms (2N4R, 2N3R) and 2N4R mutants (V248L, G272V, P301L, V337M and R406W) at a final concentration of 1  $\mu\text{M}$  with 0.5  $\mu\text{M}$  MTs at 37°C for 30 min for all the assays unless otherwise mentioned (Fig. 1b). Prior to the assay, the tau-MT solution was diluted 5-fold in the motility solution containing 10  $\mu\text{M}$  paclitaxel, 1 mM MgCl<sub>2</sub>, 1 mM ATP, 25 mM D-glucose, 216  $\mu\text{g ml}^{-1}$  glucose oxidase,

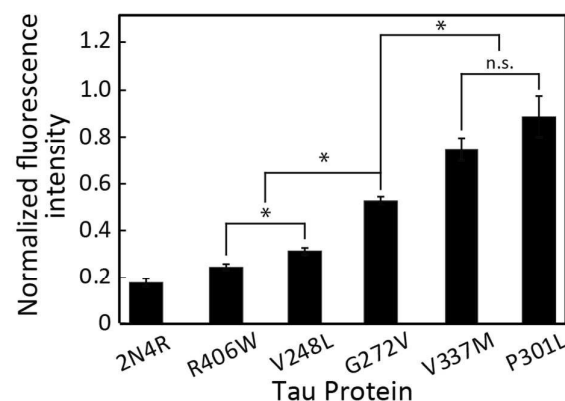


**Fig. 5.** Various 2N4R tau mutations demonstrate distinct effects on Fls. MTs incubated with wild 2N4R showed consistently lower FI than any of the five mutants analyzed. FI for R406W was significantly lower than those for V248L, G272V, V337M and P301L ( $p < 0.05$ ). FI for G272V was significantly lower than those for V337M and P301L ( $p < 0.05$ ) and higher than those for V248L and R406W ( $p < 0.05$ ), respectively. Mean  $\pm$  SEM; \*:  $p < 0.05$ ; n.s.:  $p > 0.05$  (ANOVA);  $n \geq 16$ .

36  $\mu\text{g ml}^{-1}$  catalase and 1% (v/v) of 2-mercaptoethanol in BRB80 to minimize the photobleaching effect in fluorescent imaging. MTs without tau incubation were taken as control (no tau-MT). The respective tau-bound MTs, henceforth, are called as 2N4R-MT, 2N3R-MT, V248L-MT, G272V-MT, V337M-MT, P301L-MT and R406W-MT.

#### On-chip protein assay

The pluronic surfactant-treated microfluidic device was flushed with casein solution (0.5  $\text{mg ml}^{-1}$  casein in BRB80) and incubated for 5 min at room temperature. Next, the kinesin solution was introduced and incubated for 5 min. Finally, the diluted tau-MT solution (0.1  $\mu\text{M}$  MT) was introduced and the flow cell was immediately sealed with vacuum grease (8009-03-8, APIEZON). Image acquisition was started after 5-min incubation.

#### Imaging and data processing

Fluorescence images were obtained using an inverted fluorescence microscope (IX71, Olympus, Japan) equipped with a 100 $\times$  oil immersion objective lens (UPLSAPO 100XO, Olympus) and a charge-coupled device camera (ORCA-R2, Hamamatsu, Japan). MTs were observed by epifluorescence using a 100 W mercury short-arc lamp (USH-1030L, Ushio, Japan) with a neutral density 12 filter and U-MWIG3 fluorescence filter cube. The image acquisition was performed with an exposure time of 500 ms in conjunction with the imaging system HDR-35 recording software (Hamamatsu). Images of  $86.7 \times 66.0 \mu\text{m}^2$  (1 pixel = 129 nm) were stored in 12-bit TIFF format and processed using ImageJ (National Institute of Health, USA). The background was subtracted using the Rolling-Ball background correction plugin,<sup>33</sup> then the region of interest enclosing a single collector was selected ( $220 \mu\text{m}^2$ ) and the average FI was measured. FI values

measured in three independent devices (18 assay regions) for each type of tau-MT were averaged and normalized by the FI value obtained from the control device, i.e. no tau-MT assayed device. Student's *t*-test was performed to estimate the significance of the difference between two experimental conditions. Analysis of variance (ANOVA) was applied to evaluate if the difference between the groups was statistically significant.

## Results and discussion

### MT motility in the microfluidic device

The ability of the device to carry out MT gliding assay was firstly tested using no tau-MTs. All MTs that entered microchannel reached collector without any detected U-turns. Over 94% of MTs were kept in collectors due to arrowhead shape (Table S1). MTs were concentrated within MT collectors over time (Figs. 3b and 3c), reaching saturation approximately after 25 min (Fig. 3d). The image of the overhang structure created by the same fabrication process was previously shown in Fig. 2a in Fujimoto et al.<sup>28</sup> Throughout the assay, overhang structure and selective kinesin patterning efficiently kept MTs in the assay region. None of the MTs gliding along the periphery of the assay region were able to climb out of the overhang structure (Table S2). Therefore, the conceptual device design and its application for MT gliding assay were demonstrated successfully.

### MT accumulation depends on their binding and gliding capacity over kinesin-coated surface

Measuring FI at the collectors was a simple but effective way of detecting how specific tau protein species affects MT kinesin binding and gliding. FI for 2N4R-MTs in the collector was significantly lower than that for the control even at 5 min after starting the assay (*t*-test,  $p < 0.001$ , Fig. 3d). The lower FI for 2N4R-MTs can be due to: (i) the lower landing rate and density of 2N4R-MTs (Figs. S1a and S1b) over kinesin-coated surface, shown in our previous report<sup>18</sup> resulting in a fewer MTs available for transport to the collector, (ii) the lower gliding velocity of 2N4R-MTs<sup>15,21</sup> resulting in a slower accumulation of MTs in the collector. Hence, all these parameters played their roles in regulating the amount of MTs accumulated in the collectors.

### Differentiation of 3R: 4R tau isoform ratios

The accumulation of tau-MTs with different ratios of 2N3R:2N4R; 0:1, 1:3, 1:1, 3:1 and 1:0 (with a total tau concentration of 1  $\mu$ M) is shown in Fig. 4 as normalized FIs. MTs incubated with any of the 2N3R:2N4R ratios tested here demonstrated significantly lower FIs than the control (*t*-test,  $p < 0.001$ ). Accumulation of MTs decreased with the increase of 2N4R, the FIs of 1:1, 1:3 and 0:1 were indistinguishable ( $p > 0.05$ ) and were significantly lower than 1:1 and 1:0. Further, the FI of 1:1 was significantly lower than 1:0; therefore we were able to differentiate 2N3R and 2N4R tau

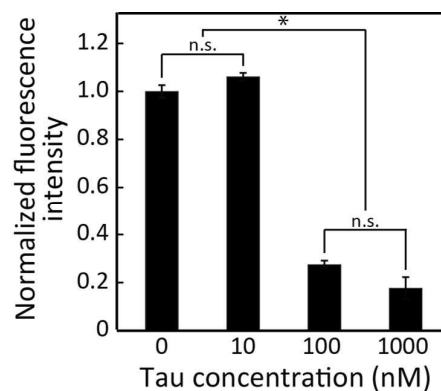


**Fig. 6.** Detection limit of the device. Significantly lower MT accumulation became apparent above 100 nM 2N4R. No significant difference with a control (no tau-MT) was noticed for 10 nM 2N4R. Mean  $\pm$  SEM; \*:  $p < 0.05$ ; n.s.:  $p > 0.05$  (ANOVA);  $n \geq 16$ .

isoforms and different ratios of them up to the ratio of 1:1 in our microfluidic device.

The effect of various 2N3R:2N4R ratios on MT accumulation can be seen, because 3R and 4R tau isoforms have a different affinity to MTs due to MTBR's net charge: 4R tau isoforms have a higher net positive charge at MTBRs, resulting in higher affinity to MTs than 3R tau isoforms (Table S3). Importantly, the higher net positive charge results in a higher steric hindrance of MT-kinesin interaction<sup>13</sup>, ultimately resulting in the less efficient binding of MTs to the kinesin-coated surface. This leads to low MT landing rate, binding density and gliding velocity.<sup>15,18,21</sup> Therefore, when the total charge of 4R tau exceeds those of 3R tau in the mixture, we were able to differentiate various 3R:4R tau ratios (Fig. 4). Certainly, the low FI in our on-chip assay recaptured the greater hindrance of 4R isoforms than 3R isoforms on the MT-kinesin interaction, as previously reported in other studies.<sup>13,15,18,21,34</sup>

### Differentiation of MTBR mutations in 2N4R tau isoform

All of the five mutant forms of 2N4R tau showed a significant increase in MT accumulation compared to wild 2N4R ( $p < 0.05$ , Fig. 5). We were able to differentiate the MTBR mutations (V248L, G272V, V337M and P301L) from non-MTBR mutation R406W (Fig. 5;  $p < 0.05$ ). Moreover, among MTBR mutations, G272V was significantly different from V337M and P301L (Fig. 5;  $p < 0.05$ ). MAPT mutations are known to alter the tau binding affinity to MTs with respect to their position in the tau structure: the affinity is decreased by mutations in MTBRs compared to those in other regions.<sup>35,36</sup> According to their locations, P301L has the most deteriorating effect on the binding affinity, followed by V337M, G272V and R406W, although the effect of V248L has not been reported yet.<sup>37</sup> Unlike MTBR mutations, the non-MTBR mutation, R406W, is known to affect the binding affinity to MTs, only when it is phosphorylated.<sup>38</sup> This might be a reason that our nonphosphorylated R406W showed lower FI compared to other MTBR mutations. Therefore, the decrease of tau binding

1 affinity corresponding to the mutation position was captured  
2 in our on-chip assay.

### 3 Tau detection limit

4 To identify the detection limit of the proposed device, we  
5 assayed lower concentrations (0 and 100 nM) of 2N4R (Fig. 6).  
6 The lowest detectable concentration was 100 nM ( $p < 0.05$ ,  
7 Fig. 6). Although our device was not optimized to detect CSF  
8 tau ( $< 14$  pM), the detection limit of 2N4R tau isoform falls into  
9 the ranges (0.2–1.0  $\mu$ M) reported by another non-immuno tau  
10 detection method.<sup>10</sup> A lower detection limit can be achieved  
11 by a trade-off with assay time. Longer assays emphasise the  
12 effect of binding and gliding for extremely low concentrations.  
13 Moreover, performing assay in a longer microchannel results  
14 in an amplified effect of the gliding velocity, which requires  
15 longer assay time. As a result, faster or more sensitive  
16 detection can be optimized depending on targeted  
17 applications.

### 18 Conclusion

19 We developed a single detection unit facilitating the analysis of  
20 the tau effect on MT-kinesin binding<sup>13,18</sup> and MT gliding<sup>15,18,23</sup>  
21 towards on-chip tau detection. The device was designed such  
22 as to emphasize the differences in MT affinity in the reservoir,  
23 MT motility in microchannel and the arrowhead collector to  
24 effectively capture the additive outcome from both these  
25 parameters. The combined effect of these parameters resulted  
26 in a higher sensitivity (~10% higher) than obtained by the off-  
27 chip measurements.<sup>18</sup> The TAT (~5 min) is shorter than in  
28 conventional tau protein detection methods (4–48 hrs).<sup>8,39</sup>  
29 Although, the sensitivity is lower than the conventional  
30 immuno-based methods,<sup>7,8</sup> it is relatively better than other  
31 non-immuno assays.<sup>10,13</sup> This method requires only a single  
32 image to determine the effect of a particular tau species,  
33 which can be more widely used than kinesin motility-based  
34 detection that necessitates velocity measurement.<sup>13</sup>  
35 The overall alteration of 3R:4R tau ratio irrespective of the  
36 type of projection domain (0N, 1N or 2N) is attributed to  
37 various neurodegenerative disorders.<sup>40</sup> Because the binding  
38 affinity of tau proteins is determined by the number of MTBRs,  
39 our assay has the potential to differentiate when 3R:4R ratio is  
40 altered by diseases. However, the next challenge to apply our  
41 device to the actual CSF sample will be a method to eliminate  
42 the influence from other coexisting proteins such as other  
43 MAPs and mutants. Thus, the current setup is still in the  
44 preclinical stage, but has the potential to be a future antibody-  
45 free detection method owing to its short assay time and easy  
46 readout. In addition, the device may also be applied for  
47 elucidation of the effect of other microtubule associated  
48 proteins (MAPs).<sup>41</sup>

### 49 Acknowledgements

50 This work is supported by Nakatani foundation (RY); Japan  
51 Society for the Promotion of Science (JSPS) (06035-123332)

(RY); JSPS and NSF under the Japan U.S. Cooperative Science  
Program (11033011-000121) (RY); NIH/NIMH 2R44MH091909  
(SLK), JSPS L-15536 (SLK), Grant-in-Aid for Scientific Research  
(KAKENHI) 26790030 (MCT), Kyoto University Supporting  
Program for Interaction-Based Initiative Team Studies (SPIRITS)  
(SPS, RY) as part of the Program for Promoting the  
Enhancement of Research Universities, the Ministry of  
Education, Culture, Sports, Science and Technology (MEXT),  
Japan.

### Reference

1. H. V. Vinters, *Annual Review of Pathology: Mechanisms of Disease*, 2015, 10, 291-319.
2. S. Schraen-Maschke, N. Sergeant, C.-M. Dhaenens, S. Bombois, V. Deramecourt, M.-L. Caillet-Boudin, F. Pasquier, C.-A. Maurage, B. Sablonniere, E. Vanmechelen and L. Buee, *Biomarkers in Medicine*, 2008, 2, 363-384.
3. B. L. Goode, M. Chau, P. E. Denis and S. C. Feinstein, *Journal of Biological Chemistry*, 2000, 275, 38182-38189.
4. K. Blennow, *NeuroRx: The Journal of the American Society for Experimental Neuro Therapeutics*, 2004, 1, 213-225.
5. H. Hampel, K. Blennow, L. M. Shaw, Y. C. Hoessler, H. Zetterberg and J. Q. Trojanowski, *Experimental Gerontology*, 2010, 45, 30-40.
6. C. M. Karch, A. T. Jeng and A. M. Goate, *Journal of Biological Chemistry*, 2012, 287, 42751-42762.
7. M. Vandermeeren, M. Mercken, E. Vanmechelen, J. Six, A. Vandevoorde, J. J. Martin and P. Cras, *Journal of Neurochemistry*, 1993, 61, 1828-1834.
8. D. Wagshal, S. Sankaranarayanan, V. Guss, T. Hall, F. Berisha, I. Lobach, A. Karydas, L. Voltarelli, C. Scherling, H. Heuer, M. C. Tartaglia, Z. Miller, G. Coppola, M. Ahljanian, H. Soares, J. H. Kramer, G. D. Rabinovici, H. J. Rosen, B. L. Miller, J. Meredith and A. L. Boxer, *Journal of Neurology Neurosurgery and Psychiatry*, 2015, 86, 244-250.
9. A. Neely, C. Perry, B. Varisli, A. K. Singh, T. Arbnesi, D. Senapati, J. R. Kalluri and P. C. Ray, *ACS Nano*, 2009, 3, 2834-2840.
10. J. O. Esteves-Villanueva, H. Trzeciakiewicz and S. Martic, *The Analyst*, 2014, 139, 2823-2831.
11. H. Nehme, S. Chantepie, J. Defert, P. Morin, D. Papy-Garcia and R. Nehme, *Analytical and Bioanalytical Chemistry*, 2015, 407, 2821-2828.
12. N. A. Verwey, W. M. van der Flier, K. Blennow, C. Clark, S. Sokolow, P. P. De Deyn, D. Galasko, H. Hampel, T. Hartmann, E. Kapaki, L. Lannfelt, P. D. Mehta, L. Parnetti, A. Petzold, T. Pirttila, L. Saleh, A. Skinningsrud, J. C. Swieten, M. M. Verbeek, J. Wiltfang, S. Younkin, P. Scheltens and M. A. Blankenstein, *Annals of Clinical Biochemistry*, 2009, 46, 235-240.
13. M. C. Tarhan, Y. Orazov, R. Yokokawa, S. L. Karsten and H. Fujita, *Lab on a Chip*, 2013, 13, 3217-3224.
14. H. Hagiwara, H. Yorifuji, R. Satoyoshitake and N. Hirokawa, *Journal of Biological Chemistry*, 1994, 269, 3581-3589.
15. A. Peck, M. E. Sargin, N. E. LaPointe, K. Rose, B. S. Manjunath, S. C. Feinstein and L. Wilson, *Cytoskeleton*, 2011, 68, 44-55.
16. A. Seitz, H. Kojima, K. Ojima, E. M. Mandelkow, Y. H. Song and E. Mandelkow, *EMBO Journal*, 2002, 21, 4896-4905.

17. C. T. Lin, M. T. Kao, E. Meyhofer and K. Kurabayashi, *Applied Physics Letters*, 2009, 95, 64.
18. S. Subramaniyan Parimalam, M. C. Tarhan, S. L. Karsten, H. Fujita, H. Shintaku, H. Kotera and R. Yokokawa, *Micro Electro Mechanical Systems (MEMS), IEEE 27th International Conference on*, 26-30 Jan. 2014, 314-317.
19. B. Trinczek, A. Ebner, E. M. Mandelkow and E. Mandelkow, *Journal of Cell Science*, 1999, 112 Pt 14, 2355-2367.
20. K. A. Butner and M. W. Kirschner, *Journal of Cell Biology*, 1991, 115, 717-730.
21. D. Yu, N. E. LaPointe, E. Guzman, V. Pessino, L. Wilson, S. C. Feinstein and M. T. Valentine, *Journal of Alzheimer's Disease*, 2014, 39, 301-314.
22. C. T. Lin, M. T. Kao, K. Kurabayashi and E. Meyhofer, *Nano Letter*, 2008, 8, 1041-1046.
23. Y. Hiratsuka, T. Tada, K. Oiwa, T. Kanayama and T. Q. Uyeda, *Biophysical Journal*, 2001, 81, 1555-1561.
24. Y. M. Huang, M. Uppalapati, W. O. Hancock and T. N. Jackson, *Biomedical Microdevices*, 2007, 9, 175-184.
25. J. Clemmens, H. Hess, R. Doot, C. M. Matzke, G. D. Bachand and V. Vogel, *Lab on a chip*, 2004, 4, 83-86.
26. L. Jia, S. G. Moorjani, T. N. Jackson and W. O. Hancock, *Biomedical Microdevices*, 2004, 6, 67-74.
27. C. T. Lin, M. T. Kao, K. Kurabayashi and E. Meyhofer, *Small*, 2006, 2, 281-287.
28. K. Fujimoto, M. Kitamura, M. Yokokawa, I. Kanno, H. Kotera and R. Yokokawa, *ACS Nano*, 2013, 7, 447-455.
29. J. Howard, A. J. Hudspeth and R. D. Vale, *Nature*, 1989, 342, 154-158.
30. R. Yokokawa, M. C. Tarhan, T. Kon and H. Fujita, *Biotechnology and Bioengineering*, 2008, 101, 1-8.
31. R. C. Williams, Jr. and J. C. Lee, *Methods in Enzymology*, 1982, 85 Pt B, 376-385.
32. A. Hyman, D. Drechsel, D. Kellogg, S. Salser, K. Sawin, P. Steffen, L. Wordeman and T. Mitchison, *Methods in enzymology*, 1991, 196, 478-485.
33. S. R. Sternberg, *Computer*, 1983, 16, 22-34.
34. M. Lu and K. S. Kosik, *Molecular Biology of the Cell*, 2001, 12, 171-184.
35. M. van Slegtenhorst, J. Lewis and M. Hutton, *Experimental Gerontology*, 2000, 35, 461-471.
36. M. Hong, V. Zhukareva, V. Vogelsberg-Ragaglia, Z. Wszolek, L. Reed, B. I. Miller, D. H. Geschwind, T. D. Bird, D. McKeel, A. Goate, J. C. Morris, K. C. Wilhelmsen, G. D. Schellenberg, J. Q. Trojanowski and V. M. Y. Lee, *Science*, 1998, 282, 1914-1917.
37. N. Matsumura, T. Yamazaki and Y. Ihara, *American Journal of Pathology*, 1999, 154, 1649-1656.
38. P. K. Krishnamurthy and G. V. W. Johnson, *Journal of Biological Chemistry*, 2004, 279, 7893-7900.
39. F. R. Petry, J. Pelletier, A. Bretteville, F. Morin, F. Calon, S. S. Hebert, R. A. Whittington and E. Planel, *PLOS ONE*, 2014, 9, 1-12, e94251.
40. C. Luk, Y. Compta, N. Magdalino, M. J. Martí, G. Hondhamuni, H. Zetterberg, K. Blennow, R. Constantinescu, Y. Pijnenburg, B. Mollenhauer, C. Trenkwalder, J. Van Swieten, W. Z. Chiu, B. Borroni, A. Cámara, P. Cheshire, D. R. Williams, A. J. Lees and R. de Silva, *Journal of Neurochemistry*, 2012, 123, 396-405.
41. A. Iyer, N. E. LaPointe, K. Zielke, M. Berdyski, E. Guzman, A. Barczak, M. Chodakowska-Zebrowska, M. Barcikowska,

S. Feinstein and C. Zekanowski, *PLOS ONE*, 2013, 8, 1-11, e76409.